RSC Advances

PAPER

View Article Online
View Journal | View Issue

Cite this: *RSC Adv.*, 2014, **4**, 10491

Laser-pulled ultralong platinum and gold nanowires†

Stephen J. Percival, Noah E. Vartanian and Bo Zhang*

Received 2nd December 2013
Accepted 31st January 2014

DOI: 10.1039/c3ra47207h

www.rsc.org/advances

We report the preparation and characterization of single platinum and gold nanowires with lengths up to 5 millimeters. Quartz-sealed platinum and gold nanowires are fabricated by drawing a short piece of the corresponding microwire using a highly reproducible laser pulling procedure. Bare metal nanowires are prepared by hydrofluoric (HF) acid etching of the quartz encapsulation. We show that these nanowires have cylindrical shape and taper down to an observed diameter as small as 10 nm for platinum and 40 nm for gold, yielding exceptionally high aspect ratios. X-ray diffraction (XRD) analysis indicates that both the gold and platinum nanowires exhibit a significant preference for development of the {111} crystal face in the axis normal to the nanowire length, whereas the {200} crystal face is nearly absent in this axis which is supported by Transmission Electron Microscopy (TEM) analysis. Quartz-sealed nanowires can be easily manipulated and arranged into complex patterns with an increasing number of contact points. Electrical properties of single nanowires were measured at nearly 0.5 mm lengths at room temperature. Each of the samples tested was found to have a resistivity approaching the bulk metal value and high observed current densities before wire failure. The grain boundary reflection coefficient was calculated on single laser-pulled nanowires to be $R = 0.616$ for gold and $R = 0.259$ for platinum.

Introduction

Metal nanowires are a widely varied group of nanomaterials finding useful applications in increasingly diverse areas.[1,2] Single, long, metal nanowires are of great interest in the study of the quasi one-dimensional properties of metal nanowires and are being widely studied for their optical[3,4] and electronic properties.[1,5,6] A number of bottom-up and top-down processes have been developed to produce such nanowires. Examples of popular bottom up processes include solution phase synthesis,[7,8] template-based electrodeposition using anodic aluminum oxide (AAO)[9–11] or track-etched polycarbonate membranes,[11–14] photolithography patterned electrochemical deposition[1,15] or electron-beam lithography (EBL) patterned electrochemical deposition[16] or physical vapor deposition[17] as well as Focused Ion Beam (FIB) fabrication.[18] Solution-based synthesis methods can produce large quantity of single crystalline nanowires with smooth surfaces, although typically are of submicron lengths. Additionally, these methods produce nanoparticle by-products and single nanowires can be difficult to isolate from a bulk solution. Lithography-based electrochemical deposition methods can produce single nanowires or their arrays that typically have rectangular cross sections.[1,15] These nanowires can be of significant length, but typically are highly polycrystalline with a large number of non-uniform grain boundaries and rough surfaces.[1,15]

Unconventional mechanical production of nanowires has not been widely investigated, but has advantages of relatively simple production steps, reduced waste of noble metals and production of easily isolated single nanowires. One such mechanical method involves inserting a larger diameter wire into a metal holder and drawing the holder through dies of decreasing size, ultimately forming encased nanowires.[19] This method can produce a single platinum nanowire with a diameter as small as 8 nm, but is a time consuming process and produces unwanted structural disorder of the resulting nanowires due to the low temperature drawing which can severely affect their functionality.[20]

Another important mechanical pulling method, called the "Taylor process", involves sealing a metal wire into a glass holder and pulling the holder down to smaller dimensions while being heated.[21] This method has been used to create Bi nanowires[22] as small as 220 nm and Au wires[23] as small as 260 nm. Through an extension of this process semiconducting nanowires encased in polymer can be made as small as 5 nm.[24]

Here, we report a top-down method similar to the Taylor process, for the easy and reproducible fabrication of mm-long single platinum and gold nanowires. These nanowires are made by sealing a small piece of microwire in quartz and pulling the quartz/metal ensemble using a laser micropipette puller. This

Department of Chemistry, University of Washington, Seattle, USA. E-mail: zhang@chem.washington.edu

† Electronic supplementary information (ESI) available: Additional XRD data on Au and Pt microwires, AFM and TEM images of Pt nanowires, SEM images of broken Au and Pt nanowires after electrical measurements and zoomed out images of the shape patterned nanowires. See DOI: 10.1039/c3ra47207h

laser pulling method uses a bench-top micropipette puller, which is commercially available, to produce ultralong and continuous metal nanowire in a few seconds. The nanowires are completely sealed in quartz and can be easily released by HF acid etching. This method not only reduces amounts of materials used but also produces wires having a low degree of structural disorder due to the elevated temperatures used in the pulling procedure and is demonstrated by this investigation. Using both TEM and XRD we show that these nanowires are highly crystalline and well ordered. Electrical measurements demonstrate that such nanowires possess resistivity comparable to the bulk metals with high current densities before failure. The quartz encasement offers added mechanical stability enabling easy handling and manipulation of mm-long metal nanowires. This is demonstrated by arranging single nanowires into desired patterns on silicon substrates. This unique nanowire platform can be useful for a variety of increasingly complex applications, including new chemical sensors,[25] surface enhanced Raman spectroscopy (SERS),[9] and nanowire catalysis research.[12]

Experimental

Chemicals and materials

All chemicals and materials were used as received from the manufacturers. Deionized water (>18 MΩ cm, Barnstead Nanopure Systems), acetone (Mallinckrodt Baker), isopropyl alcohol (IPA, Mallinckrodt Baker), 25 μm platinum wire (99.95%, Alfa Aesar), gold wire (99.99%, Kurt J. Lesker), hydrofluoric acid (HF, 48 wt% conc. Sigma Aldrich), silicon wafers double side polished (Silicon Quest International Inc.), polished quartz wafers (http://UniversityWafer.com), carbon coated Formvar copper TEM grids (Ted Pella).

Physical vapor deposition (PVD)

Gold pellets (99.999%, Kurt J. Lesker) were placed in tungsten metal evaporation boats and used in the metal evaporator along with chromium coated tungsten rods (99.999%, Kurt J. Lesker) for deposition of electrical contacts using an in-house two source PVD system.

Electrical measurements

Linear sweep current–voltage response was recorded using an EG&G 175 voltage programmer and an EG&G 173 potentiostat. The current–voltage data was recorded using an in-house LabView 8.5 program on a desktop PC equipped with a PCI-6251 (National Instruments) card.

Scanning electron microscopy (SEM) and energy dispersive X-ray spectroscopy (EDS)

SEM images were obtained using a field-emission SEM (FEI Sirion). Only wires used to obtain electrical measurements were sputter coated with a ~2 nm of gold/palladium alloy or carbon for SEM imaging. EDS data was obtained using an Oxford X-max 80 mm^2 Silicon Drift Detector.

Atomic force microscopy (AFM)

AFM was performed using a Veeco Dimension 3100 AFM in tapping mode using OTESPA cantilever tips. The microscope was placed within a noise and vibration isolation table and images have been flattened to remove the background curvature of the substrate surface, but are otherwise free of modification.

X-ray diffraction (XRD)

XRD was performed using a Bruker D8 Discover system using copper Kα X-rays. Bare nanowires were etched out of the quartz on a small silicon chip. Upwards of 80 nanowires of both platinum and gold were used to collect the XRD information.

Transmission electron microscopy (TEM)

TEM imaging was performed on a FEI Technai G2 F20 S-Twin operating at 200 kV using a single tilt sample holder.

Results and discussion

Fabrication of nanowires

As illustrated in Scheme 1, the platinum and gold nanowires were mechanically pulled using a laser puller (P-2000, Sutter Instrument Co.). A similar pulling procedure can also be used to make platinum nanoelectrodes.[26–28] Briefly, a 25 μm platinum wire was placed in a quartz capillary (outer diameter: 1 mm, inner diameter: 0.3 mm) and one end sealed closed using a hydrogen flame. The platinum microwire was sealed in quartz with laser heating under vacuum. The Pt/quartz ensemble was then pulled (heat = 750, filament = 2, velocity = 60, delay = 140, pull = 250) resulting in two sharp quartz tips with the platinum nanowires sealed inside. Changing the pulling parameters may give smaller or more uniform diameters in the nanowires but may also lead to an increased incidence of breaks in the nanowire.

The gold nanowires required a slightly modified procedure because of its lower melting point, 1064 °C compared to 1768 °C for platinum. The high temperatures needed to melt the quartz (1670 °C) in order to seal the wire would inevitably melt the gold forming discrete beads to minimize its surface tension[29]

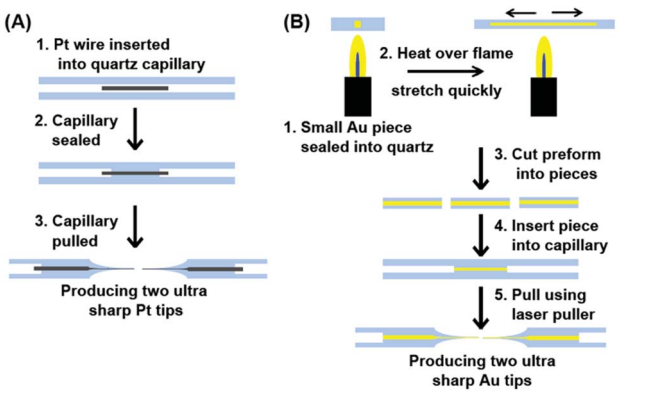

Scheme 1 (A) Fabrication of platinum nanowires and (B) gold nanowires by a laser assisted mechanical pulling method.

resulting in discontinuous sections. A piece of gold microwire preform already sealed in quartz would be made using a hand pulling method.[21,30,31] A 1 cm-long piece was placed in a quartz capillary and pulled with laser. This method, not requiring the initial laser sealing step, utilizes slightly different parameters (heat = 725, filament = 3, velocity = 100, delay = 110, pull = 225).

The tips were then broken off and placed on a silicon chip. Silicon was chosen for its resistance to HF etching and for easiness in SEM analysis, allowing the imaging without metal sputter coating, but other materials such as polyimide could also be used. The nanowire tips were then chemically etched with HF resulting in a single, ultralong (typically 4–5 mm) nanowire (**Caution**: HF acid is hazardous, use appropriate safety equipment). The nanowires were either left on the silicon for the XRD and SEM studies or transferred to different substrates using a "wedging" technique.[32]

Characterization of laser-pulled nanowires

This method allows for easy and consistent preparation of continuous nanowires over their entire length. Fig. 1 shows typical examples of laser-pulled single nanowires. Due to the nature of the pulling process, these wires are tapered and the diameter will vary over the length of the wire. For example, the platinum wire shown in Fig. 1A and B is ~10 nm diameter at the narrow tip, and ~860 nm at the opposite end. This change in diameter over the length of the wire shown, ~3 mm, means the wire decreases in diameter by ~2.8 Å μm^{-1}. Fig. 1C and D show the length and diameter for a gold nanowire where the length is ~2.7 mm and the tip diameter is ~40 nm and ~3 μm at the opposite end. The diameter at the tip of the gold nanowire is typically larger than the platinum wire due to the lower melting temperature of gold.

XRD was utilized to determine the crystal faces present in these nanowires. To perform XRD, upwards of 80 nanowires, for each gold and platinum, were placed in a semi-random orientation on silicon chips. While not quite the same as powder diffraction XRD experiments it is very similar, and the resulting diffraction peaks will be from the numerous randomly arranged crystal orientations parallel to the Si substrate (crystal face axis oriented normal to the nanowire lengths). Fig. 2 shows the XRD results for laser-pulled nanowires and delineates several characteristic diffraction peaks and their corresponding Miller indices. It is clear that the {111} crystal face is the most abundant crystal face perpendicular to the nanowire lengths. Also shown, directly below the XRD spectra, are the expected diffraction peak intensities for the respective crystal faces from a bulk platinum or gold sample. Interestingly, the {200} peak is nearly absent from the diffraction spectra for both the metal nanowires. When compared to XRD scans of commercially available 25 μm diameter Au and Pt wires (ESI Fig. S2†), which are used to make the nanowires, there is a clear reduction of the {200} peak in going from the microwire to the nanowires. Both metals have the Face Center Cubic (FCC) crystal structure where the {111} crystal face has the lowest surface energy relative to any of the other faces.[33,34] The FCC {200}, being equivalent to the FCC {100} crystal face, is known to poses the lowest strain energy of the crystal faces.[35] The large {111} peak and the limited faceting of the {200} crystal face with respect to the axis normal to the nanowire length, show that during the high temperature pulling process the metal nanowire will prefer to minimize its surface energy with respect to the quartz interface while strain energy is not minimized.

From the X-ray diffraction data an estimate of the average crystallite size was calculated for both the Au and Pt nanowires using the Scherrer equation and assuming a spherical geometry for the crystallite shapes[36,37]

$$d = \frac{K\lambda_{\mathrm{diff}}}{\omega \cos\theta} \quad (1)$$

where d is the average crystallite size, K is a constant (0.94 used for spherical crystallites of FCC crystal structure), λ_{diff} is the

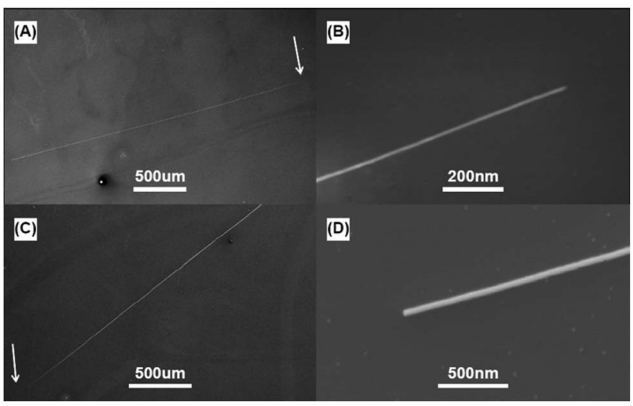

Fig. 1 SEM images showing (A) a 3 mm-long platinum nanowire and (B) the ~10 nm tip of the same wire located at the arrow in (A). SEM images showing a 2.7 mm-long gold nanowire (C) and (D) the ~40 nm tip located at the arrow shown in (C).

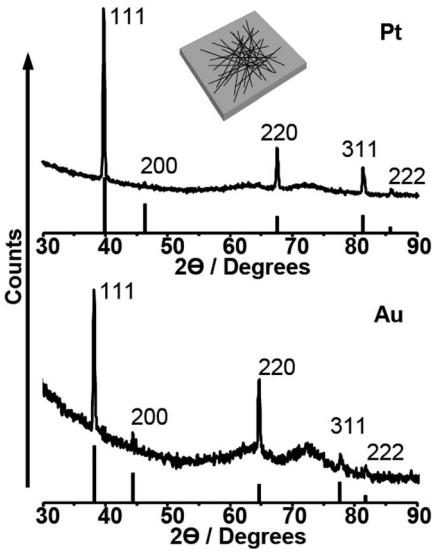

Fig. 2 XRD data from both platinum and gold nanowires: included is a schematic showing the semi random nanowire distribution on the silicon chips. The expected intensities of each crystal reflection are shown below the nanowire XRD data for comparison.

Table 1 Average crystal grain diameter sizes for laser-pulled nanowires obtained using the Scherrer equation and the two prominent XRD peaks

	Grain size (nm)	Grain size (nm)
XRD reflections	Gold	Platinum
{111}	62.8	63.1
{220}	61.4	62.4
Average	62.1	62.7

wavelength of the X-rays (copper Kα = 1.5418 Å), θ is the diffraction angle, in radians. The peak line width of the X-ray diffraction peak, ω, is measured in radians at the FWHM of the diffraction peak and will increase in width as the thickness of the crystallites decreases. The average crystallite size obtained for the two most prominent diffraction peaks are summarized in Table 1.

For both types of metal nanowires the average grain size is approximately 62 nm which is larger than the grain sizes for the precursor 25 μm diameter wires (ESI†). This increase in crystallite size is due to the high temperatures used in the pulling step which anneals the wires leading to the increase in grain size. There is evidence, from the TEM images, that the crystallites length is not dependant on the diameter of the nanowire. A representative TEM image of the end of a platinum nanowire, Fig. 3A, shows that even as the nanowire diameter decreases below the average crystallite size the lengths of the crystallites don't shorten as the wire diameter decreases. When the nanowire diameter is below the average crystallite size, it appears that the nanowire can be thought of as a chain of single crystal domains linked end to end.

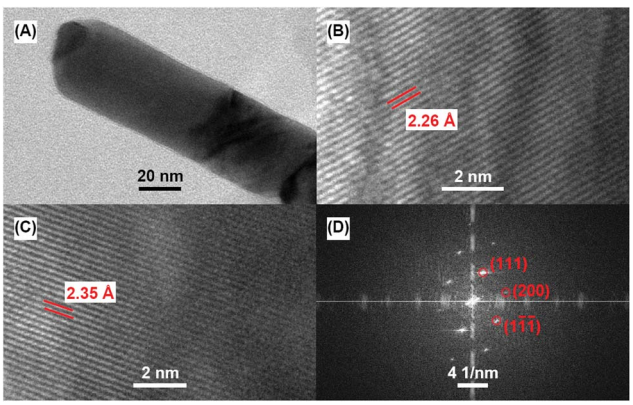

Fig. 3 (A) TEM image of a laser-pulled 40 nm diameter platinum nanowire tip where the width is seen to be comprised of single crystal domains with crystallites on either side. (B and C) TEM images of nanowires showing the atomic lattice spacing of the {111} crystal planes for (B) platinum and (C) gold. (D) FFT of the gold wire TEM image in (C) showing the reciprocal space of the [01−1] zone axis with the spatial frequencies corresponding to the (111), (1−1−1) and the (200) reflections circled. Note: the scale bar in (B) is larger than the scale bar in (C) despite both representing a 2 nm length and is the reason the spacing for the gold atomic lattice appears closer than the platinum lattice.

To further investigate the structural characteristics of the nanowires and to confirm the {111} crystal face is dominant in the axis perpendicular to the wire length, TEM was used to identify and measure the atomic lattice spacing of the respective metal wires. Fig. 3B and C show the TEM images of the sides of a platinum and gold nanowire, respectively, where the {111} crystal lattice was observed at the edges of both metal wires. The lattice spacing's were determined from the reduced Fast Fourier Transform (FFT) images and the reduced FFT for the gold nanowire is shown in Fig. 3D which corresponds to the [01−1] zone axis. For the {111} crystal face a spacing of 2.355 Å is expected for gold[38] and 2.26 Å for platinum.[39] The experimental value of the lattice spacing closely matched the literature values and further demonstrates that the atomic lattices of the nanowires are not significantly strained from the pulling process. Both the XRD and TEM data show the {111} face is the dominant face normal to the length of the wire suggesting that the {200} crystal face is more abundant in the direction parallel to the length of the wire, which could explain why the {200} XRD reflections are much weaker than expected.

Nanowire device patterns

A unique aspect of laser-pulled metal nanowires is that they can be easily handled and manipulated to form patterns and designs of increasing complexity. This is demonstrated in Fig. 4, which shows how the nanowires can be placed on top of each other to form electrical connections. A crossing point made out

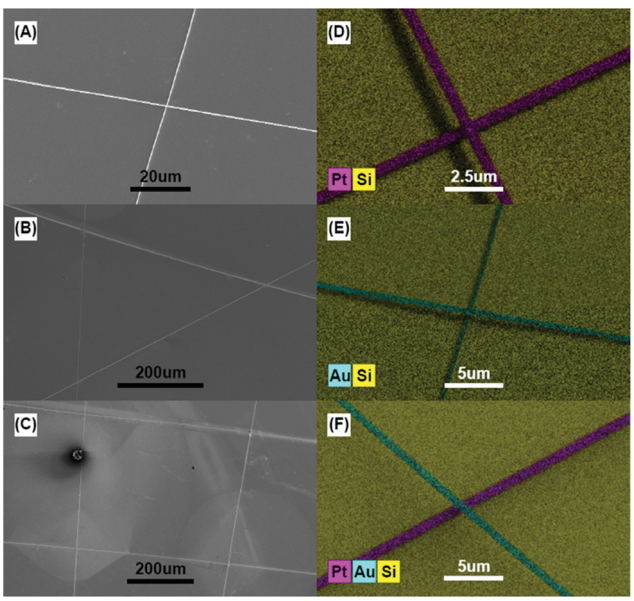

Fig. 4 SEM images of gold nanowires arranged in more complex arrangements. (A) A cross made from two gold wires forming a single contact point. (B) A triangle made from three gold nanowires forming three contact points. (C) A "pound sign" made from four gold nanowires forming four contact points between them. EDS color plots of platinum and gold nanowires contacting each other showing the versatility of the wires; (D) Pt–Pt, (E) Au–Au, and (F) Pt–Au contact points. The "shadow" seen in A and B is due to the EDS detector offset from the electron beam.

of two gold wires can be seen in Fig. 4A and designs with three and four crossing gold wires are shown in Fig. 4B and C respectively. These configurations, while being relatively simple, demonstrates the versatility of the these nanowires and one could imagine insulating some wires, patterning and exposing specific portions of the wires, and placing the connecting wires on top of the exposed contacts thereby forming basic circuits. Also illustrated in Fig. 4 are EDS images of different combinations of nanowires on silicon. Fig. 4D shows a contact point between two platinum nanowires to create a single junction. Alternatively, the wires could be gold or a combination of metal nanowires as shown in 4E and 4F, respectively. Specific combinations of metal nanowires could be placed into desired positions to achieve a type of hybrid chemical sensor where a specific combination of metal nanowires may be more sensitive for a specific analyte than a single metal alone.

Electrical measurement

The evaluation of the electrical properties of these nanowires is very important if they are to be used in any sort of electronic device or sensor. Therefore, representative single nanowires for both metals were transferred onto gold contact pads separated by ~500 μm distance and the *I–V* curves measured for each metal nanowire. The ~500 μm spacing between contacts was chosen because it was desirable to show the electrical properties of these nanowires measured over long lengths, which resulted in the use of relatively larger diameter nanowires. Due to the wedging transfer process it was difficult to transfer smaller diameter nanowires onto the contact pads that were unbroken over the 500 μm lengths. Fig. 5A shows a single Au nanowire spanning the 500 μm length between the contacts and Fig. 5B is an SEM image of the same nanowire after measurements were performed showing that the wire is now broken.

The *I–V* curve for the platinum nanowire is shown in Fig. 5D, where the current is seen to suddenly drop, quickly followed by a total current loss, indicating a break occurred in the nanowire. Interestingly, the nanowire broke on the reverse potential scan after the voltage (and hence the current) had surpassed the value where it ended up failing. The sudden breakage of the wire could be due to electromigration or may indicate the presence of defects in the nanowire where a build-up of thermal energy generated by resistive heating may have caused the wire to slightly crack followed by an arcing of the current past the crack, thus completely severing the wire. Evidence for the dramatic breakdown can be seen in Fig. 5B which shows that the gold nanowire has dramatically moved relative to its initial position and the broken end of the wire is seen to have experienced significant melting (magnified image in ESI Fig. S5†). Both ends of the broken Pt wire can be seen in Fig. 5C and shows that substantial melting of the nanowire occurred indicating a dramatic localized resistive heating or electrical arcing just after the breakage. Evidence that electromigration also played a role in the severing of the wires is seen where a thinning of the wire is observed in the magnified SEM images of the platinum wire (shown in the ESI Fig. S5†). The wire is seen to have regions of alternating thickness indicating the migration of the platinum atoms leading to the thinning and eventual breakage of the wire.

The nanowire dimensions were measured from the SEM images where the radius was determined as the average of multiple measurements taken along the measured length between contacts. Assuming a cylindrical shape with circular cross sectional area, the resistivities and current density for the gold (~487 μm length and ~342 nm radius) and platinum (~484 μm length and ~406 nm radius) nanowires was calculated. From the largest observed currents for each nanowire, the current densities observed were 2.24×10^{10} A m^{-2} for the gold nanowire and 3.25×10^{9} A m^{-2} for the platinum.

Fig. 6 shows the linear portions of the *I–V* curves from a single platinum and gold nanowire (same wires as in Fig. 5) from which the resistances of the single nanowires was determined from the slopes of the lines. The platinum nanowire showed a total resistance of 119 Ω whereas the gold wire had a

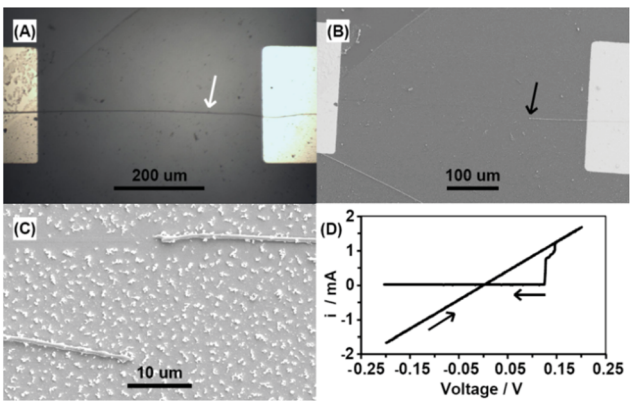

Fig. 5 (A) Optical microscope image of a single gold nanowire extending across the gap between two electrical contacts, the arrow indicates the approximate point where the wire broke during electrical measurements as seen from the SEM image of the same wire in (B). (C) SEM image of a platinum nanowire after breakage occurred showing the wire had melted and possibly arced from the current. (D) *I–V* curve for the platinum wire where after scanning the potential up to 0.2 Volts and reversing scan direction the wire experienced a partial breakage at approximately 0.148 V followed by complete breakage at 0.127 V, arrows denote scan direction.

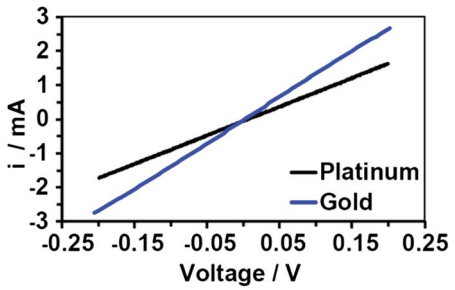

Fig. 6 Linear portion of the *I–V* curves from −0.2 to 0.2 Volts for both the platinum and gold wires which were used to evaluate the electrical properties of the nanowires.

resistance of 74 Ω. The resistivity of each nanowire was then determined using eqn (2).

$$R = \frac{\rho L}{A} \quad (2)$$

Where R is the electrical resistance of the measured nanowire, ρ is the resistivity, L is the length of the measured nanowire between the electrical contacts and A is the cross sectional area. Assuming a circular cross sectional area, the resistivity of the Au nanowire was 5.59×10^{-8} Ω m and 1.27×10^{-7} Ω m for the Pt nanowire. These values are close to the bulk resistivity values of the metals at room temperature being 2.255×10^{-8} Ω m for Au and 1.06×10^{-7} Ω m for Pt.[40]

Metal nanowires are expected to have higher resistivities than bulk metals, which can be attributed to scattering of the conduction electrons from the surfaces[7] and grain boundaries,[41] as well as the normal scattering due to lattice vibrations and impurity sites. Conduction electrons can scatter elastically from the surface where there will be no loss of momentum, termed specular reflection, and has been described by Fuchs[42] and Sondheimer.[43]

The contribution of surface scattering of conduction electrons to the total resistivity increases as the wire diameter decreases due to an increase in the surface/volume ratio. Thus, the larger diameter of these nanowires means that the largest contribution to the resistivity due to electron scattering comes from the scattering at crystal grain boundaries in the nanowires and can be calculated using the Mayadas and Shatzkes model.[44,45] The Mayadas and Shatzkes model of grain boundary scattering has been extended by Steinhoegl and coworkers[46,47] to include the surface scattering contributions from Fuchs and Sondheimer theory

$$\rho = \rho_o \left(\frac{1/3}{\left[\frac{1}{3} - \frac{\alpha}{2} + \alpha^2 - \alpha^3 \ln\left(1 + \frac{1}{\alpha}\right)\right]} + C(1-p)\left(\frac{U}{S}\right)\lambda \right) \quad (3)$$

where $\alpha = \left(\frac{\lambda}{d}\right)\left(\frac{R_{GB}}{1 - R_{GB}}\right)$, ρ is the measured resistivity, ρ_o is the bulk metal resistivity, C is a constant (3/16 in the case for a circular wire cross section[48]), d is the crystal grain diameter, λ is the electron mean free path length (23 nm for Pt[49] and 41 nm for Au[50]), p is the probability of elastic surface scattering ($p = 1$ is totally specular scattering and $p = 0$ is totally diffuse), and U and S are the circumference and cross sectional area of the nanowire respectively. R_{GB} is the reflection coefficient for electrons to scatter at the grain boundaries in the metal nanowire which for these wires will contribute most to the resistivity. The surface scattering will be small as compared to the grain boundary scattering, for these diameter wires, so taking a value of p that is similar to that reported previously will allow an approximate calculation of R_{GB}. Taking $p = 0.5$, which has been reported previously by Durkan and coworkers,[41] and solving for the grain boundary reflectance coefficient is an appropriate assumption where specular surface scattering has been reported as high as ~0.85 for Au {111} surface.[51] The resistivities of these nanowires, being close to that of the bulk metals, could mean that a majority of the electrons flowing through the wire are scattered elastically from the surface and that there is a low probability of being diffusely reflected from a grain boundary. Using these simple assumptions grain boundary reflection coefficients of 0.616 and a low 0.259 have been calculated for the gold and platinum wire respectively. The Pt reflection coefficient is quite low indicating a low probability of grain boundary reflection and in fact is not far from previous reports of 0.35 for Pt thin films.[49]

Interestingly, the gold nanowire I–V curve, seen in Fig. 7A, began to show nonlinearity at higher bias voltages and the nonlinear current–voltage behavior becomes more pronounced at higher potentials. This behavior may be due to a temperature increase resulting from Ohmic heating leading to a resistance increase.[16] Assuming a linear relationship, the increase in resistivity as the temperature of the nanowire increases can be expressed as the simple relation known as Mattheisen's rule

$$\rho = \rho_o[1 + \alpha_{TCR}(T - T_o)] \quad (4)$$

where ρ_o is the wire resistivity at a reference temperature, T_o, 25 °C in this case, T is the temperature of the metal nanowire, and α_{TCR} is the temperature coefficient of resistivity for the given material being 3.715×10^{-3} °C^{-1} for Au.[15,40] By using this simple assumption, the changing resistivity can be used to calculate the temperature of the wire. Fig. 7B shows the inferred temperature for the gold wire as a function of the voltage biased across the wire. As the bias potential is scanned from −1 to 0 Volts, the nanowire temperature decreases to a minimum (the room temperature value ~25 °C), and the nanowire resistivity decreases to its room temperature value. Scanning from 0 up to +1 Volts, the resistivity again begins to increase and this resistivity change corresponds to an inferred temperature of over 850 °C without the nanowire breaking. SEM images of the broken ends of the gold nanowire, seen in the ESI,† do show

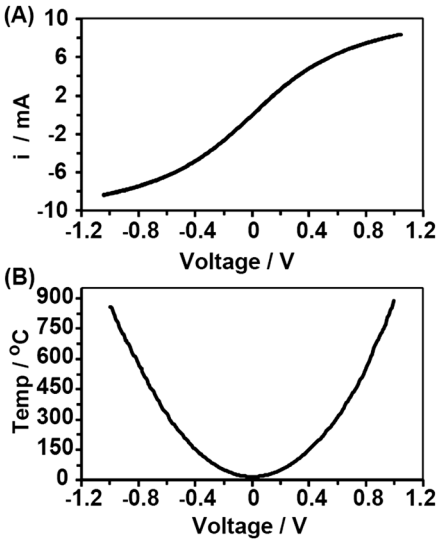

Fig. 7 (A) I–V curve for a gold nanowire showing the current nonlinearity at higher potentials, and (B) the inferred temperature of the gold nanowire as a function of voltage due to Ohmic heating, taken from the resistance change seen in (A).

evidence of substantial heating where the wire has melted and lead to failure of the wire.

Conclusions

Millimeter-long single metal nanowires have been prepared using a laser pulling method. These laser pulled nanowires have unsurpassed aspect ratios and are highly crystalline with low structural disorder. Additionally, the process used to make these nanowires appears to produce wires that favor low surface energy crystal faces normal to the length of the wire as exemplified by the {111} crystal face for gold and platinum, which are both FCC crystals. XRD data confirms that the wires are polycrystalline with crystal grains of approximately 62 nm in diameter, on average. TEM analysis allowed the atomic lattice spacing to be measured and verifies that the atomic lattice is not highly strained from the pulling procedure. These nanowires can be easily manipulated to make increasingly complex patterns that can be incorporated into functional nano-devices utilizing combinations of the metal nanowires. The nanowires exhibit a very low resistivity approaching that of the bulk metals and also showed fairly high current densities before wire failure. At higher voltages the gold wire displayed a nonlinear current response that may be explained as an increasing resistance due to Ohmic heating. The reflection coefficient for the nanowires was calculated to be 0.616 for gold and a remarkably low 0.259 for platinum.

This nanowire preparation method is simple and highly reproducible. Single metal nanowires fabricated with this method have very high aspect ratios and can be easily manipulated and incorporated into nano-devices. These metal nanowires can be used as a unique platform for nanowire-based chemical and biological sensors or for studying catalytic reactions on single nanowires. Both gold and platinum nanowires have been made although other metals may also be used with this procedure. Future studies will be done to investigate the conductance of smaller diameter nanowires as well as two crossed nanowires to investigate the nature of the conductance of the point where the wires touch, as it may form an atomic scale conductor.

Acknowledgements

The authors are grateful for the financial support from the Defense Threat Reduction Agency (DTRA) (Contract no. HDTRA1-11-1-0005). Part of this work was conducted at the University of Washington NanoTech User Facility, a member of the National Science Foundation, National Nanotechnology Infrastructure Network (NNIN) and the Washington Technology Center (WTC).

Notes and references

1 C. Xiang, Y. Yang and R. M. Penner, *Chem. Commun.*, 2009, 859–873.
2 S. Banerjee, A. Dan and D. Chakravorty, *J. Mater. Sci.*, 2002, **37**, 4261–4271.
3 S. Lal, J. H. Hafner, N. J. Halas, S. Link and P. Nordlander, *Acc. Chem. Res.*, 2012, **45**, 1887–1895.
4 E. J. R. Vesseur, R. de Waele, M. Kuttge and A. Polman, *Nano Lett.*, 2007, **7**, 2843–2846.
5 J.-Y. Lee, S. T. Conner, Y. Cui and P. Peumans, *Nano Lett.*, 2008, **8**, 689–692.
6 C. Wang, Y. Hu, C. M. Lieber and S. Sun, *J. Am. Chem. Soc.*, 2008, **130**, 8902–8903.
7 B. J. Wiley, Z. Wang, J. Wei, Y. Yin, D. H. Cobden and Y. Xia, *Nano Lett.*, 2006, **6**, 2273–2278.
8 Z. Xu, C. Shen, S. Sun and H.-J. Gao, *J. Phys. Chem. C*, 2009, **113**, 15196–15200.
9 J. Baik, S. J. Lee and M. Moskovits, *Nano Lett.*, 2009, **9**, 672–676.
10 K. Skinner, C. Dwyer and S. Washburn, *Nano Lett.*, 2006, **6**, 2758–2762.
11 C. R. Martin, *Science*, 1994, **266**, 1961–1966.
12 C. Koenigsmann, E. Sutter, R. R. Adzic and S. S. Wong, *J. Phys. Chem. C*, 2012, **116**, 15297–15306.
13 S. Karim, K. Maaz, G. Ali and W. Ensinger, *J. Phys. D: Appl. Phys.*, 2009, **42**, 185403.
14 G. De Marzi, D. Lacopino, A. J. Quinn and G. Redmond, *J. Appl. Phys.*, 2004, **96**, 3458–3462.
15 E. J. Menke, M. A. Thompson, C. Xiang, L. C. Yang and R. M. Penner, *Nat. Mater.*, 2006, **5**, 914–919.
16 H. X. He, S. Boussaad, B. Q. Xu, C. Z. Li and N. J. Tao, *J. Electroanal. Chem.*, 2002, **522**, 167–172.
17 C. Durkan, M. A. Schneider and M. E. Welland, *J. Appl. Phys.*, 1999, **86**, 1280–1286.
18 P. Shi, J. Zhang, H.-Y. Lin and P. W. Bohn, *Small*, 2010, **6**, 2598–2603.
19 A. C. Sacharoff, R. M. Westervelt and J. Bevk, *Rev. Sci. Instrum.*, 1985, **56**, 1344–1346.
20 A. C. Sacharoff, R. M. Westervelt and J. Bevk, *Phys. Rev. B: Condens. Matter Mater. Phys.*, 1982, **26**, 5976–5979.
21 G. F. Taylor, *Phys. Rev.*, 1924, **23**, 655–660.
22 E. F. Skelton, J. D. Ayers, S. B. Qadri, N. E. Moulton, K. P. Cooper, L. W. Finger, H. K. Mao and Z. Hu, *Science*, 1991, **253**, 1123–1125.
23 H. K. Tyagi, H. W. Lee, P. Uebel, M. A. Schmidt, N. Joly, M. Scharrer and P. St. J. Russell, *Opt. Lett.*, 2010, **35**, 2573–2575.
24 J. J. Kaufman, G. Tao, S. Shabahang, D. S. Deng, Y. Fink and A. F. Abouraddy, *Nano Lett.*, 2011, **11**, 4768–4773.
25 F. Yang, S.-C. Kung, M. Cheng, J. C. Hemminger and R. M. Penner, *ACS Nano*, 2010, **4**, 5233–5244.
26 B. B. Katemann and W. Schuhmann, *Electroanalysis*, 2002, **14**, 22–28.
27 Y. Li, D. Bergman and B. Zhang, *Anal. Chem.*, 2009, **81**, 5496–5502.
28 Y. Shao, M. V. Mirkin, G. Fish, S. Kokotov, D. Palanker and A. Lewis, *Anal. Chem.*, 1997, **69**, 1627–1634.
29 K. K. Nanda, A. Maisels and F. E. Kruis, *J. Phys. Chem. C*, 2008, **112**, 13488–13491.
30 K. Han, J. D. Embury, J. J. Petrovic and G. C. Weatherly, *Acta Mater.*, 1998, **46**, 4691–4699.

31 V. S. Larin, A. V. Torcunov, A. Zhukov, J. González, M. Vazquez and L. Panina, *J. Magn. Magn. Mater.*, 2002, **249**, 39–45.
32 G. F. Schneider, V. E. Clado, H. Zandbergen, L. M. K. Vandersypen and C. Dekker, *Nano Lett.*, 2010, **10**, 1912–1916.
33 C. V. Thompson and R. Carel, *Mater. Sci. Eng., B*, 1995, **32**, 211–219.
34 L. Vitos, A. V. Ruban, H. L. Skriver and J. Kollár, *Surf. Sci.*, 1998, **411**, 186–202.
35 J.-M. Zhang, K.-W. Xu and V. Ji, *Appl. Surf. Sci.*, 2002, **185**, 177–182.
36 P. Scherrer, *Göttinger Nachrichten Math. Phys.*, 1918, **2**, 98–100.
37 H. Borchert, E. V. Shevchenko, A. Robert, I. Mekis, A. Kornowski, G. Grübel and H. Weller, *Langmuir*, 2005, **21**, 1931–1936.
38 Y. Q. Wang, W. S. Liang and C. Y. Geng, *Nanoscale Res. Lett.*, 2009, **4**, 684–688.
39 L. L. Kesmodel and G. A. Somorjai, *Phys. Rev. B: Solid State*, 1975, **11**, 630–637.
40 *CRC Handbook of Chemistry and Physics*, ed. D. R. Lide, CRC Press, Boca Raton FL, 86th edn, 2005
41 C. Durkan and M. E. Welland, *Phys. Rev. B: Condens. Matter Mater. Phys.*, 2000, **61**, 14215–14218.
42 K. Fuchs, *Proc. Cambridge Philos. Soc.*, 1938, **34**, 100–108.
43 E. H. Sondheimer, *Adv. Phys.*, 1952, **1**, 1–42.
44 A. F. Mayadas and M. Shatzkes, *Phys. Rev. B: Solid State*, 1970, **1**, 1382–1389.
45 A. F. Mayadas, M. Shatzkes and J. F. Janak, *Appl. Phys. Lett.*, 1969, **14**, 345–347.
46 W. Steinhoegl, G. Schindler, G. Steinlesberger, M. Traving and M. Engelhardt, *Proceedings of the 2003 International Conference on Simulation of Semiconductor Processes and Devices*, 2003, p. 27.
47 W. Steinhögl, G. Schindler, G. Steinlesberger and M. Engelhardt, *Phys. Rev. B: Condens. Matter Mater. Phys.*, 2002, **66**, 075414.
48 R. B. Dingle, *Proc. R. Soc. London, A*, 1950, **201**, 545–560.
49 Q. G. Zhang, B. Y. Cao, X. Zhang, M. Fujii and K. J. Takahashi, *J. Phys.: Condens. Matter*, 2006, **18**, 7937–7950.
50 J. A. Johnson and N. M. Bashara, *J. Appl. Phys.*, 1967, **38**, 2442–2446.
51 J. R. Sambles, K. C. Elsom and D. J. Jarvis, *Philos. Trans. R. Soc. London, Ser. A*, 1982, **304**, 365–396.

